crystals

MDPI

Article

First-Principles Electronic-Structure Study of Graphene Decorated with 4*d*-Transition Atoms

Ran Hu [1], Wei-Chao Zhang [2] and Wei-Feng Sun [2,*]

[1] Shenzhen Power Supply Bureau Co., Ltd., China Southern Power Grid, Shenzhen 518000, China; huran@sz.csg.cn
[2] Key Laboratory of Engineering Dielectrics and Its Application, Ministry of Education, School of Electrical and Electronic Engineering, Harbin University of Science and Technology, Harbin 150080, China; weichao.zhang@hrbust.edu.cn
* Correspondence: sunweifeng@hrbust.edu.cn; Tel.: +86-158-4659-2798

Abstract: Adsorption configurations, electronic structures and net spins of graphene adsorbing 4*d* transition atoms are calculated by first-principles calculations to explore the magnetic modification of decorating metal atoms on graphene. Y, Zr and Nb atoms can be adsorbed on graphene sheet via ionic bonds with an evident charge transfer, while Mo, Tc, Ru and Rh atoms form covalent-like bonding with graphene carbon atoms due to orbital hybridization, as indicated by Mulliken atomic charges and electron density differences. The 4*d*-transition atoms can be adsorbed on a carbon-ring center and atomic-bridge with a high binding energy as the typical chemisorption, which leads to specific modifications in electronic-band character and magnetic properties by introducing electron-states near Fermi-level. By adsorbing 4*d*-transition atoms, the electronic structure of graphene will alter from a semi-metal to a metal character, and engender net spin magnetism from the spin-polarization in 5*s* and 4*d* orbitals of adsorption atoms. This paper provides a significant theoretical basis for further experimental explorations of the atom-decorated graphene in nanoelectronics.

Keywords: graphene; transition metal; adsorption configuration; first-principles calculation

Citation: Hu, R.; Zhang, W.-C.; Sun, W.-F. First-Principles Electronic-Structure Study of Graphene Decorated with 4*d*-Transition Atoms. *Crystals* **2021**, *11*, 29. https://doi.org/10.3390/cryst11010029

Received: 19 December 2020
Accepted: 28 December 2020
Published: 30 December 2020

1. Introduction

In recent years, graphene has regained major attention for prospective applications of nanoscience and condense physics due to its distinctive electronic structure and excellent mechanical and thermal properties [1–4]. The sp^2 hybrid bonding in the carbon atom plane and the large conjugated π bond formed by vertical p_z orbitals make graphene exhibit non-magnetic semi-metal electrical properties [3]. In particular, graphene represents a linear energy dispersion of electronic-states near the Fermi-level to engender a Dirac cone electronic structure. A diversity of exquisite graphene nanostructures obtained through elaborate nanotechnology processes has been successfully applied for chemical catalysts, energy storage mediums, nanoelectronic and spintronic devices, and gas detectors [5–11]. Through specific processing schemes, graphene can achieve comprehensive functions to further extend its practical applications. Electrical conductivity could be effectively modified by adjusting the width of graphene nanoribbons [12,13]. Recent literature reports have noted that several frontier works are focusing on exploring nanomeshed and doping-decorated graphene for modifying electronic structures [14–16].

At present, considerable progress has been made in theoretical research on graphene adsorption of metal atoms. Valencia performed first-principles calculations on the atomic structure, adsorption binding energy and molecular-orbital caused magnetism of the graphene and single-wall carbon nanotubes (SCNT) adsorbed by 3*d*-transition atoms, which proved the stable and dispersive adsorptions of Sc, Ti, Fe and Co atoms on graphene sheet without surface migration [17]. Yagi used theoretical methods to investigate the stable configurations and magnetic properties of the graphene and SCNT adsorbing Fe, Co and Ni

atoms, indicating that an electronic transition from 4*s*-orbital to 3*d*-orbital of the adsorbed atoms results in an evident decrease of the magnetic moment [18]. It has been theoretically demonstrated that the main group I−III metal atoms can be adsorbed on the graphene surface by ionic bonds as manifested by the large charge transfer, which leads to a slight change in electronic states, while the transition metal, noble metal and main group IV atoms are capable of forming covalent bonds with the graphene carbon atomic-layer through strong orbital hybridization [19]. By adsorbing main group IV atoms, graphene wills from semi-metallic to metallic characters and acquires a magnetic moment from the localized *p*-orbital of IV atoms [20]. With the projected augmented wave method of first-principles calculations, Sun elucidated the metallic band-structure and the *s*-orbital derived magnetism of the graphene being adsorbed with alkali metal atoms [21]. It has been also reported that Mg and Ca atoms can be adsorbed on graphene sheet by using van der Waals interaction and ionic bonding, respectively [22]. Ataca investigated hydrogen storage performances of graphene adsorbed with Ca atoms by the pseudopotential plane-wave first-principles method, suggesting that chemical adsorption of Ca atoms on graphene surface leads to the metallic character of electrical conductance [23]. Furthermore, it was proposed that applying planar strains on graphene could efficiently increase the adsorption binding energy of Ca atoms on graphene [24].

There are a variety of adsorbable elements for graphene decorations which can be fulfilled by the advanced nanotechnologies recently used for graphene adsorption experiments. Therefore, new functions can be realized by graphene adsorption of atoms or molecules to provide a promising route for nano-applications. Although the low spin-orbit coupling of carbon and the long-term spin-coherence residing in graphene promise favorable applications in spintronics, the non-magnetic behaviors of pristine graphene are the first obstacle to overcome. Controllable spin magnetism can be introduced by bombarding graphene with electron and ion beams to produce regulated defects [25–27]. Recent theoretical works focus on introducing controllable magnetic orders by creating defects into graphene, such as doping substitutional 4*d* and 5*d*-transition atoms in graphene, which however are poorly feasible in fabrication processes [28,29]. In contrast, atomic-decoration of chemically adsorbing magnetic *d*-transition atoms start-up a practical route to realize controllable magnetism in graphene. Up to now, adsorbing 4*d*-transition metals on a graphene surface has not been comprehensively reported in literature. After being intrigued by the significant research with a prospective deliberation, in the present study, we pursue theoretical calculations of the adsorption configuration, binding energy electronic structure and magnetic characteristics with the pseudopotential plane-wave first-principles method to reveal the adsorption behavior and magnetic generation mechanism.

2. Calculation Methodology

Conforming to the pseudopotential plane-wave first-principles method based on spin density functional theory, the atomic structure, electronic structure and magnetic moment of single-layered graphene adsorbed with 4*d*-transtion atoms are calculated as implemented in CASTEP code of the Materials Studio v2017R2 (Accelrys Inc., San Diego, CA, USA) software package. Gradient corrected exchange-correlation functional in WC form is adopted to perform the spin-polarized calculations, with the up and down spin states being modeled by different wave-functions according to relativistic Dirac equations [30]. The interactions between atomic-cores and electrons are described by On-the-fly Generation Ultrasoft Pseudopotential, which incorporates the Koelling-Harmon scheme for treating relativistic effects [31]. Electronic wave-functions are expanded by plane-wave basis-set with an energy cutoff of 440.0 eV, in which the Smart algorithm is used to decrease the error of basis-set finiteness to an adequately low level [32]. Self-consistent field (SCF) iterations are carried out with a convergence tolerance of 5×10^{-7} eV/atom in a FFT grid of $72 \times 72 \times 216$ to ensure the accuracy of electron density calculations, in which the Pulay scheme of density mixing in charge and spin magnitudes of 0.5 and 2.0, respectively, is utilized to realize electron relaxations [33,34]. The $\boldsymbol{k}$ point sampling of integrating on the

Brillouin zone (BZ) is carried out on a Monkhorst-Pack 4 × 4 × 1 grid [35]. The geometry optimization for relaxing adsorption configurations is performed by minimizing energy-functionality with the BFGS algorithm in delocalized internal coordinates to reach an energy convergence of 5.0×10^{-6} eV/atom, with the atomic force and stress being less than 0.02 eV/Å and 0.001 Å, respectively [36].

A monolayer graphene model is constructed in 3-dimensions by setting a sufficiently thick vacuum layer (30 Å) between the periodic-imaged graphene layers so that the actual representation is a two-dimensional system of single-layer graphene. The 4 × 4 × 1 graphene supercell with a larger size along graphene atomic-plane is constructed with one 4*d*-transition atom being added for a modeling adsorption system, in which no interaction should be considered between the adsorbed atoms in adjacent periodic units. The adsorption binding energy (adsorption energy) is derived by subtracting the total energy of adsorption configuration from the total energy summation of individual 4d-transition atoms and single-layered graphene.

3. Results and Discussion

3.1. Adsorption Energy and Configuration

According to the hexagonal symmetry of graphene, the decoration atoms may be adsorbed on the tops of three positions: a carbon atom, C-C bond middle and carbon-ring center, which are nominated here by atom (A), bridge (B) and central (C) sites, as schematically shown in Figure 1. The space symmetry group of graphene is $D_{6H\text{-}1}$, which transforms into $C_{3V\text{-}1}$, $C_{S\text{-}1}$ and $C_{6V\text{-}1}$ symmetries while adsorbing atom on A, B and C sites, respectively. The 4*d*-transition atoms are introduced individually at the three adsorption sites of graphene sheet. The equilibrium adsorption structures are obtained by geometric optimizations of the first-principles total energy minimization to evaluate the adsorption energy and the geometrical distortion of graphene sheet. In order to reveal the charge transfer and Coulomb interaction between the adsorbed atoms and graphene sheet, Mulliken atomic charges are calculated for charge population analyses according to SCF electron density.

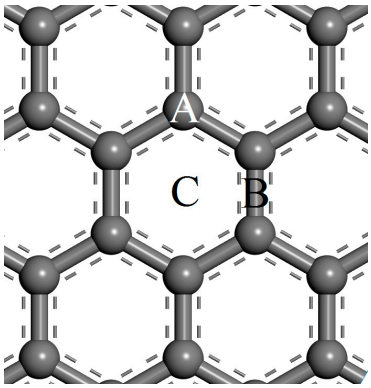

Figure 1. Three adsorption sites of metal atoms on graphene: the Atomic-carbon site (A), Bridge site (B) and Center site (C).

Adsorption energy (E_{ad}) and adsorption distance $d_{ad} = z_{ad} - z_{ave}$ (z_{ad} and z_{ave} indicate the z coordinates of adsorbed atoms and the average z coordinates of graphene carbon atoms, the coordinate axis of which is perpendicular to graphene sheet in the initial model), warpage of graphene sheet (Δc), Mulliken charges (q_M/e) of adsorbed atoms and net spin ($s_n/(\hbar/2)$) of adsorption systems are obtained by first-principles calculations with the results being listed in Table 1. All the 4*d*-transition atoms represent the highest and lowest adsorption energies at C and B sites, respectively. Pd, Ag and Cd atoms adsorbed on various sites show lower relative adsorption energies than other 4*d*-transition atoms, which are below the lower limit of ~1.6 eV of typical chemisorptions and hereby imply the physical interactions through van der Waals force [37]. Significant electron transfers between the adsorbed Y, Zr and Nb atoms and graphene adsorbent, as indicated by large

q_M, manifest the chemical adsorption through ionic bonding which is more consistent with the higher adsorption energies than with 1.7 eV, even at the B site. In contrast, Mo, Tc, Ru and Rh atoms are adsorbed on graphene by forming a covalent bond with graphene carbon atoms through orbital hybridization, as manifested by the apparently smaller q_M and the high adsorption energy that is similar to for Y, Zr and Nb atoms, which agree well with the recent reports of first-principle calculations [19]. Furthermore, adsorption energy rises with the increase of the atomic number for Mo,Tc,Ru/graphene adsorptions. A larger q_M identifies more charge transfers and indicates a stronger Coulomb interaction of ion bonding, while a longer adsorption distance indicates a weaker adsorbing action. In comparison with the Y element, the q_M and d_{ad} of the Zr atom adsorbed on A or C sites are smaller when reaching the highest adsorption energy in all 4*d*-transistion elements, thereby suggesting that q_M and d_{ad} coordinately affect adsorption strength. Pd, Ag and Cd atoms are adsorbed on graphene in a distance that is remarkably longer than the chemical bonding distance between atoms, especially exceeding 3.0 Å for Ag and Cd. For chemisorptions, the longest adsorption distance coincides with the lowest adsorption energy at the B site compared with the other two adsorption sites. The adsorbed atoms on the graphene surface causes the deviation of the nearby carbon atoms out to the other side of the graphene adsorption surface, resulting in warping deformation of the fully planar graphene, which can be described by the graphene sheet warpage $\Delta c = z_{min} - z_{ave}$ (z_{min} and z_{ave} denote the minimum and averaged coordinates of the *z*-axis vertical to the graphene sheet). Additionally, 4*d*-transition atomic-adsorptions on the A site distort the largest warpage of the graphene sheet, thereby approaching the highest Δc value of 0.555 Å. A larger Δc implies more covalent components in adsorption bonding, which is basically consistent with q_M results.

Table 1. Adsorption energy (E_{ad}/eV), adsorption distance to the graphene sheet (d_{ad}/Å), warpage of graphene sheet (Δh/Å), Mulliken charge (q_M/e) populated on transition atom, net spin ($s_n/(\hbar/2)$) of single-layer graphene adsorbing 4*d*-transition metal atoms on atomic-carbon (A), bridge (B) and center (C) sites, respectively.

	Site	E_{ad}/eV	d_{ad}/Å	Δc/Å	q_M/e	$s_n/(\hbar/2)$		Site	E_{ad}/eV	d_{ad}/Å	Δc/Å	q_M/e	$s_n/(\hbar/2)$
	A	2.763	1.687	−0.555	1.32	0		A	3.213	1.652	−0.320	0.65	0
Y	B	1.735	2.055	−0.212	0.76	0	Ru	B	2.095	2.063	−0.032	0.41	2.00
	C	3.028	1.727	−0.214	1.42	0		C	3.817	1.542	−0.126	0.58	0
	A	4.313	1.496	−0.473	1.25	1.23		A	2.169	1.863	−0.110	0.47	0
Zr	B	2.026	2.088	−0.148	0.60	3.87	Rh	B	1.663	2.091	−0.031	0.34	1.00
	C	4.770	1.586	−0.205	1.37	0		C	2.249	1.666	−0.068	0.46	0
	A	2.670	1.652	−0.480	0.99	1.87		A	1.956	2.202	−0.070	0.34	0
Nb	B	1.830	2.184	−0.018	0.48	4.89	Pd	B	1.452	2.151	−0.051	0.25	0
	C	3.363	1.520	−0.224	1.06	0		C	1.570	2.019	−0.026	0.34	0
	A	1.840	1.770	−0.298	0.74	2.58		A	0.729	2.605	−0.067	0.27	0
Mo	B	1.793	2.290	−0.029	0.35	5.18	Ag	B	0.242	3.083	−0.004	0.05	1.00
	C	2.148	1.469	−0.210	0.69	0		C	0.484	2.501	−0.030	0.24	0
	A	2.095	1.541	−0.477	0.55	0		A	0.505	3.526	−0.044	0.01	0
Tc	B	1.936	2.144	−0.038	0.39	3.01	Cd	B	0.207	3.569	−0.009	0.07	0
	C	3.147	1.470	−0.176	0.56	0		C	0.508	3.541	−0.031	0.01	0

The adsorption characteristics can also be explained by electron ionization potentials of metal atoms on graphene surface. The first electron ionization potential (IP) of 4*d*-transition atoms are calculated with the same first-principles method as for graphene adsorbing systems by E^+-E (E^+ and E represent the total energies of the positively charged cations with +e and the neutral atoms respectively in vacuum). The IP values of Pd, Ag and Cd atoms are 8.62, 8.97, 9.05 eV, respectively, which are appreciably higher than 5.66, 5.92 and 6.57 eV of Y, Zr and Nb, respectively, while Mo, Tc, Ru and Rh atoms possess medium IP values of 7.15, 7.50, 7.73 and 7.82 eV, respectively. Therefore, 4*d*-orbital electrons of Pd, Ag and Cd atoms can hardly transfer to or participate in covalent bonding with graphene carbon, leading to a physical adsorption, while the other 4d-transition atoms

show a possible capacity for chemisorptions by forming ionic or covalent bonds with the graphene sheet. In comparison with the adsorption energies of three sites on the graphene sheet for adsorbing 4*d*-transition atoms, the C site can present the highest adsorption energy to form the most stable adsorption configuration the highest locating probability, while showing a zero net spin. Therefore, we only consider the chemical absorption on the C site in the following analyses of adsorption bonding characteristics and band-structures without spin-splitting in the next section. Nevertheless, Zr, Nb, Mo and Tc/graphene B-site adsorptions present a substantial net spin higher than 3.0($\hbar/2$) resulting from 4*d*-orbital sin-polarization, which is specifically investigated with the spin-dependent partial density of states (PDOS) in the following Section 3.3 to elucidate their dominant attributes of spin magnetism.

3.2. Adsorption Bonding Characteristics

To reveal the bonding characteristics of 4*d*-transition atoms adsorbed on graphene, electron density differences (EDD) are derived from SCF electron density in space distributions being contoured on the over-atomic plane perpendicular to graphene sheet, as shown by the color maps in Figure 2. For Y and Zr atoms being adsorbed at the C site, the lowest negative EDD appears around the adsorbed atoms along the direction towards the carbon ring center (the C site center), implying that a significant electron transfer from Y and Zr to the graphene sheet occurs as a manifestation of the ionic bonding character. For Nb atoms, the lowest negative EDD region shift to the route towards carbon atoms of the benzene ring at the C site, thereby undertaking a certain orientation of electron transfer as a trend towards covalent bond characteristics. In contrast, Mo, Tc, Ru and Rh atoms adsorbed at the C site present the highest positive and lowest negative EDD regions, respectively, along the ways to the benzene center and the adjacent carbon atoms of the C-site, therefore showing an obvious directionality of the characteristic covalent bonding in the localized electronic states. The charge population analyses based on the Muliken algorithm verify that the oxidation states of Mo, Tc, Ru and Rh atoms adsorbed on the graphene sheet are much less than the lowest oxidation states of oxide compounds, as listed in Table 1, therefore confirming their covalent characteristics of chemisorptions.

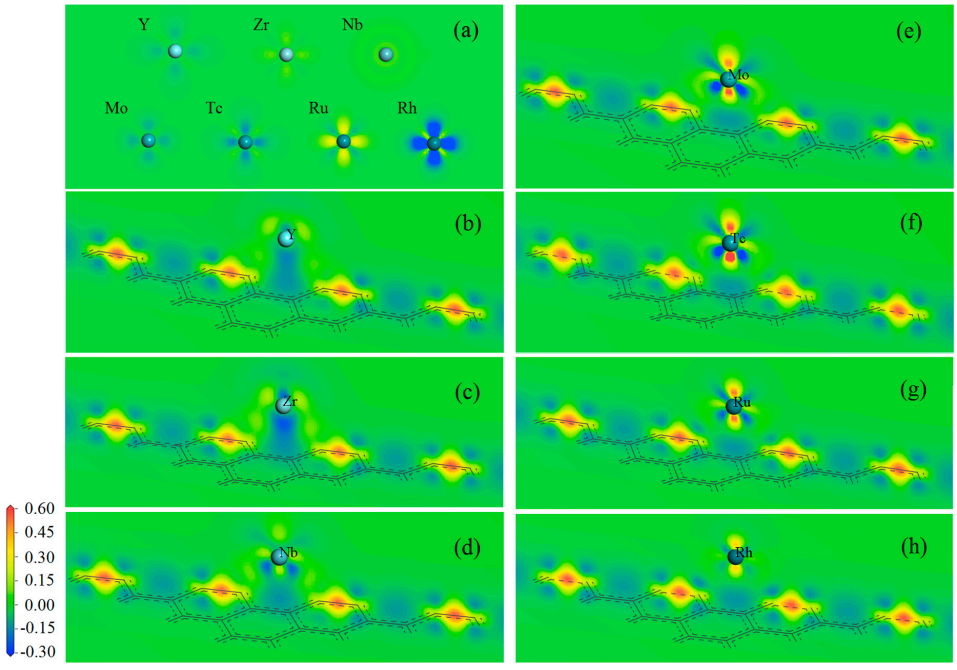

Figure 2. Electron density differences of (**a**) isolated 4*d*-transition atoms and (**b**–**h**) Y, Zr, Nb, Mo, Tc, Ru and Rh/graphene C-site adsorptions, contoured on the plane vertical to the graphene sheet and crossing the absorbed atom.

3.3. Band Structure and Magnetism

Since the influence of physically adsorbed atoms on the graphene electronic structure is negligible, the electronic structure calculations are merely performed for Y, Zr, Nb, Mo, Tc, Ru and Rh/graphene chemisorptions on the most stable C-site, as shown by the band-structure results in Figure 3. No spin-polarization has been found in the band structure of pristine graphene with a zero density of states at the Fermi-level, which confirms the non-magnetic semi-metallic character of graphene which is consistent with the results reported in other research [36,37]. The band-structures of Y, Zr and Nb/graphene C-site adsorptions retain the Dirac point of graphene, while the Fermi-level has been shifted to a higher energy due to the electron transfer from the adsorbed atoms, which also introduces the unoccupied σ* localized states above the Fermi-level. It is noted that the energy level of the lowest energy σ* state moves closer to the Fermi-level with the increase of the atomic-number. After individually adsorbing Y, Zr and Nb atoms at the C-site, the band-structure of graphene alters from semi-metallic to metallic characteristics, after which the electron transfer from the adsorbed atoms to graphene matrix leads to the π* band crossing the Fermi-level as a manifestation of n-type doping characteristics. By contrast, the occupied σ states below the Fermi-level are introduced into the band-structures of Mo,Tc,Ru,Rh/graphene adsorptions, implying that the adsorption atom has formed a covalent bond with graphene.

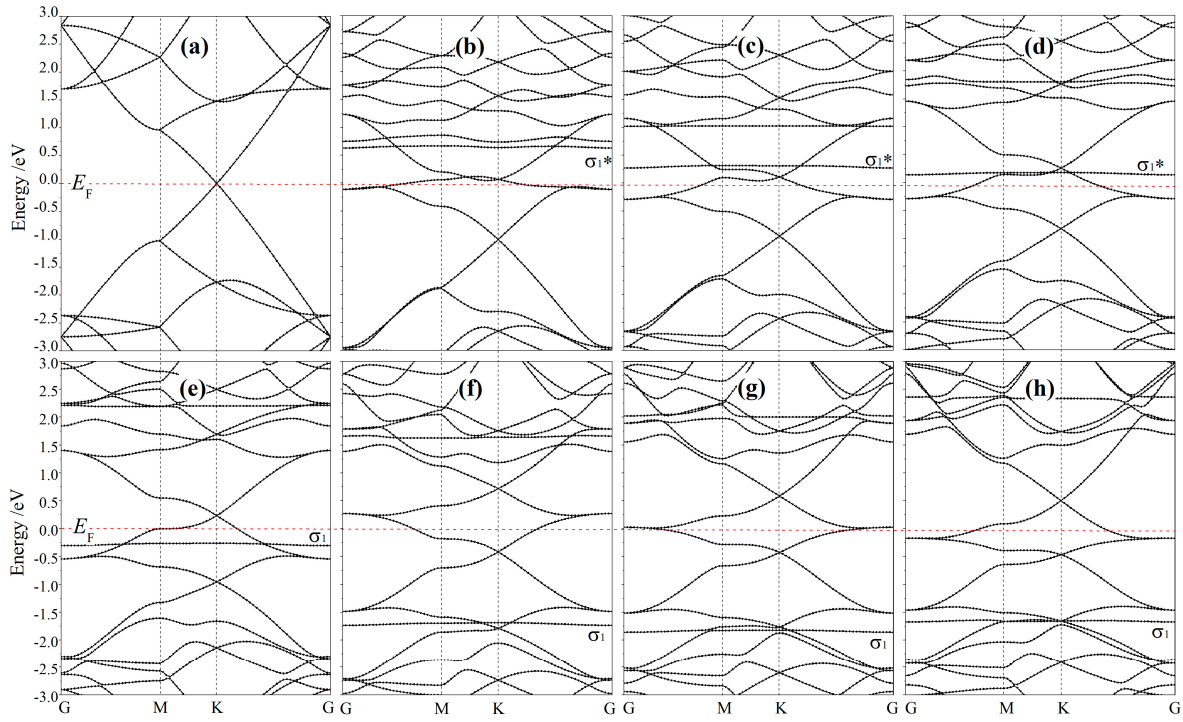

Figure 3. Electronic band structure and density of states for (**a**) pristine graphene and (**b**–**h**) Y, Zr, Nb, Mo, Tc, Ru, Rh/graphene C-site adsorptions, respectively. The Fermi-level is referenced as energy zero (horizontal dashed lines).

For the B-site chemisorptions of 4d-transition atoms on graphene sheet, spin polarization breaks the spatial symmetry distribution between the up (α) and down (β) spin states, which leads to electronic energy splitting (spin splitting) and a net spin magnetic moment, as shown in Table 1. Zr, Nb, Mo and Tc/graphene B-site adsorptions represent the substantial net spins of 3.87, 4.89, 5.18 and 3.01(ħ/2), respectively, which originate from the spin-polarization of 4*d* and 5*s* orbitals in the adsorbed atoms, as illustrated by spin-the resolved partial density of states (SPDOS) in Figure 4. For Zr and Nb/graphene adsorptions, the energy levels of β-states from 5*s* and 4*d* orbitals have been increased above the Fermi-level while the remaining α-states from 4*d* orbital are occupied below the

Fermi-level, thereby indicating that spin polarization splits the energy levels of α and β spin-states, which leads to a higher density of α-state electrons than β-state electrons and thus produces a net spin. In Mo and Tc/graphene adsorptions, the α-states and β-states are respectively dominated by Mo-5*s* and Tc-4*d* orbitals located at the Fermi-level that are partially occupied, while the exacerbation of spin-polarization further splits the majorities of 4*d*-orbital α and β states to be respectively lower and higher than the Fermi-level by 0.3 eV. Therefore, B-site Mo and Tc atoms are adsorbed on graphene by forming *s*-*p* and *d*-*p* covalent bonds respectively with the conjugated π bond derived from C-2*p* orbitals, as indicated by the minorities of Mo-5*s* α-states and Tc-4*d* β states just below the Fermi-level with the net spin being increased and decreased, respectively. To this end, the Zr, Nb, Mo and Tc/graphene B-site adsorptions represent a substantial magnetic moment that is essentially contributed to by the spin-polarized electrons from 5*s* and 4*d* orbitals of the adsorbed atoms.

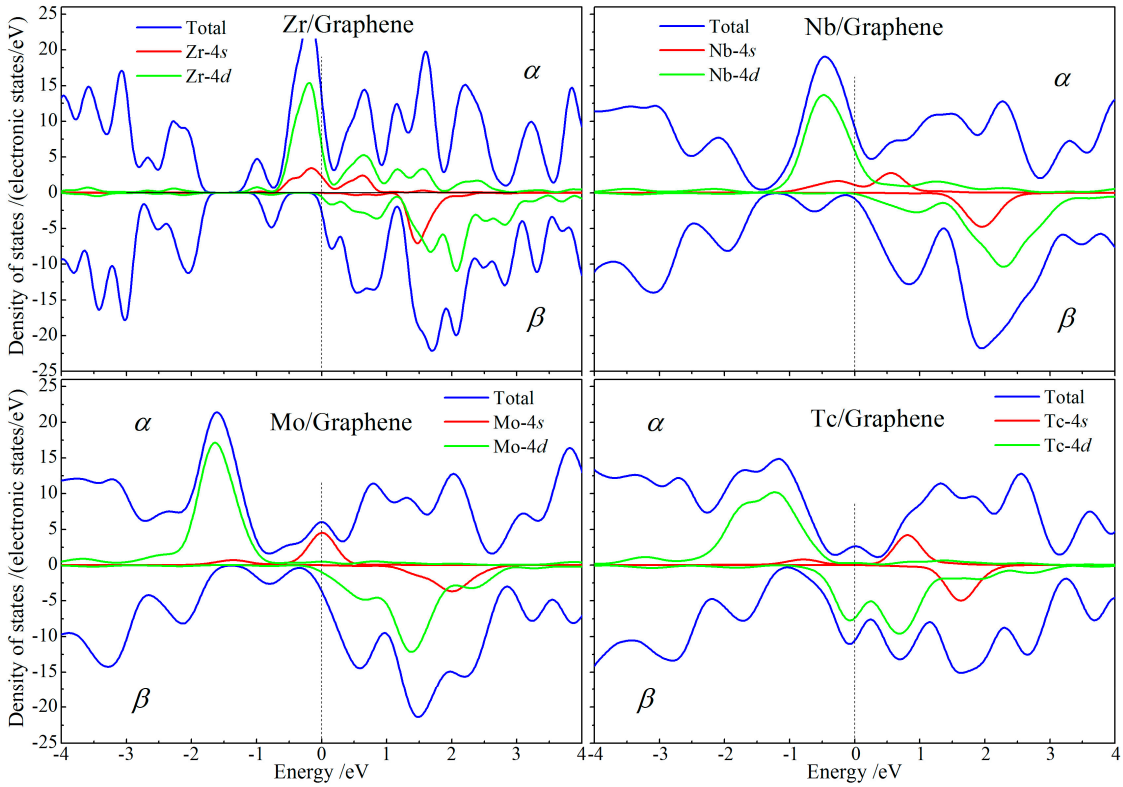

Figure 4. Spin-dependent partial density of states (PDOS) of Zr, Nb, Mo and Tc/graphene B-site adsorptions with the Fermi-level (vertical dash line) being referenced as energy zero and a Gaussian smearing of 0.1 eV.

4. Conclusions

The atomic geometry, electronic structure and magnetic properties of 4*d*-transition atoms adsorbed on graphene sheet are studied by using first principle calculations. Except for the physical adsorptions of Pd, Ag and Cd atoms on graphene, Y, Zr, Nb and Mo, Tc, Ru and Rh atoms could be chemically adsorbed with the most stable configuration at the central site of graphene by ionic and covalent bonds, respectively. The adsorptions of 4*d*-transition atoms by ionic bonds are similar to the n-type doping in graphene, leading to a fundamental transformation of the electronic structure from semi-metallic to metallic band characters, which is attributed to the significant elevation of the Fermi-level caused by the effective electron transfer from adsorbed atoms to graphene. The C-cite chemisorptions of 4*d*-transition atoms represent a clear Dirac point in the band-structure, while the significant net spin magnetism can only be acquired by B-site chemisorptions. Spin-resolved partial density of states indicate that the net spin essentially derives from the spin-splitting

of 5*s*-orbital in ionic Coulomb adsorption and 4*d*-orbital in covalent bonding adsorption. The present study demonstrates that the electronic and magnetic properties of graphene can be effectively regulated by doping 4*d*-transition atoms of Y, Zr, Nb, Mo, Tc, Ru and Rh to form stable chemisorptions, which provides a theoretical basis for applying the atomic-decorated graphene in nanoelectronics.

Author Contributions: Conceptualization, W.-F.S.; Data curation and Formal analysis, R.H.; Investigation and Writing, W.-F.S.; Project administration, W.-C.Z. All authors have read and agreed to the published version of the manuscript.

Funding: This research was funded by the National Natural Science Foundation of China (Grant No. 51337002).

Informed Consent Statement: Informed consent was obtained from all subjects involved in the study.

Data Availability Statement: Calculation methods and results are available from the authors.

Conflicts of Interest: The authors declare no conflict of interest.

References

1. Castro Neto, A.H.; Peres, N.M.R.; Novoselov, K.S.; Geim, A.K. The electronic properties of graphene. *Rev. Mod. Phys.* **2009**, *81*, 109–162. [CrossRef]
2. Balandin, A.A.; Ghosh, S.; Bao, W.; Calizo, I.; Teweldebrhan, D.; Miao, F.; Lau, C.N. Superior thermal conductivity of single-layer graphene. *Nano Lett.* **2008**, *8*, 902–907. [CrossRef] [PubMed]
3. Novoselov, K.S.; Geim, A.K.; Morozov, S.V.; Jiang, D.; Katsnelson, M.I.; Grigorieva, I.V.; Dubonos, S.V.; Firsov, A.A. Two-dimensional gas of massless Dirac fermions in graphene. *Nature* **2005**, *438*, 197–200. [CrossRef] [PubMed]
4. Lee, C.; Wei, X.; Kysar, J.W.; Hone, J. Measurement of the elastic properties andintrinsic strength of monolayer graphene. *Science* **2008**, *321*, 385–388. [CrossRef] [PubMed]
5. Li, Y.; Zhou, Z.; Yu, G.; Chen, W.; Chen, Z. CO catalytic oxidation on iron-embedded graphene: Computational quest for low-cost nanocatalysts. *J. Phys. Chem. C* **2010**, *114*, 6250–6254. [CrossRef]
6. Pumera, M. Graphene-based nanomaterials for energy storage. *Energ. Environ. Sci.* **2011**, *4*, 668–674. [CrossRef]
7. Kaukonen, M.; Krasheninnikov, A.V.; Kauppinen, E.; Nieminen, R.M. Doped graphene as a material for oxygen reduction reaction in hydrogen fuel cells: A computational study. *ACS Catal.* **2013**, *3*, 159–165. [CrossRef]
8. Liao, L.; Lin, Y.C.; Bao, M.; Cheng, R.; Bai, J.; Liu, Y.; Qu, Y.; Wang, K.L.; Huang, Y.; Duan, X. High-speed graphene transistors with a self-aligned nanowire gate. *Nature* **2010**, *467*, 305–308. [CrossRef]
9. Lin, Y.M.; Dimitrakopoulos, C.; Jenkins, K.A.; Farmer, D.B.; Chiu, H.Y.; Grill, A.; Avouris, P. 100-GHz Transistors from wafer-scale epitaxial graphene. *Science* **2010**, *327*, 662. [CrossRef]
10. Yazyev, O.V.; Katsnelson, M.I. Magnetic correlations at graphene edges: Basis for novel spintronics devices. *Phys. Rev. Lett.* **2008**, *100*, 047209. [CrossRef]
11. Schedin, F.; Geim, A.K.; Morozov, S.V.; Hill, E.W.; Blake, P.; Katsnelson, M.I.; Novoselov, K.S. Detection of individual gas molecules adsorbed on graphene. *Nat. Mater.* **2007**, *6*, 652–655. [CrossRef]
12. Ma, L.; Wang, J.; Ding, F. Strain-induced orientation-selective cutting of graphene into graphene nanoribbons on oxidation. *Angew. Chem. Int. Ed.* **2012**, *51*, 1161–1164. [CrossRef] [PubMed]
13. Ma, L.; Wang, J.; Ding, F. Recent progress and challenges in graphene nanoribbon synthesis. *Chem. Phys. Chem* **2013**, *14*, 47–54. [CrossRef] [PubMed]
14. Xiu, S.L.; Zheng, M.M.; Zhao, P.; Zhang, Y.; Liu, H.Y.; Li, S.J.; Chen, G.; Kawazoe, Y. An effective method of tuning conducting properties: First-principles studies on electronic structures of graphene nanomeshes. *Carbon* **2014**, *79*, 646–653. [CrossRef]
15. Santos, E.J.; Sánchez-Portal, D.; Ayuela, A. Magnetism of substitutional Co impurities in graphene: Realization of single π vacancies. *Phys. Rev. B* **2010**, *81*, 125433. [CrossRef]
16. López-Corral, I.; Germán, E.; Juan, A.; Volpe, M.A.; Brizuela, G.P. DFT study of hydrogen adsorption on palladium decorated graphene. *J. Phys. Chem. C* **2011**, *115*, 4315–4323. [CrossRef]
17. Valencia, H.; Gil, A.; Frapper, G. Trends in the adsorption of 3*d* transition metalatoms onto graphene and nanotube surfaces: A DFT study and molecular orbital analysis. *J. Phys. Chem. C* **2010**, *114*, 14141–14153. [CrossRef]
18. Yagi, Y.; Briere, T.M.; Sluiter, M.H.; Kumar, V.; Farajian, A.A.; Kawazoe, Y. Stable geometries and magnetic properties of single-walled carbon nanotubes doped with 3*d* transition metals: A first-principles study. *Phys. Rev. B* **2004**, *69*, 075414. [CrossRef]
19. Chan, K.T.; Neaton, J.; Cohen, M.L. First-principles study of metal adatom adsorption on graphene. *Phys. Rev. B* **2008**, *77*, 235430. [CrossRef]
20. Gao, H.J.; Zhou, M.; Lu, M.; Fa, W.; Chen, Y. First-principles study of the IVA group atoms adsorption on graphene. *J. Appl. Phys.* **2010**, *107*, 114311. [CrossRef]
21. Sun, M.; Tang, W.; Ren, Q.; Wang, S.; Yu, J.; Du, Y.; Zhang, Y. First-principles study of the alkali earth metal atoms adsorption on graphene. *Appl. Surf. Sci.* **2015**, *356*, 668–673. [CrossRef]

22. Liu, X.; Wang, C.Z.; Hupalo, M.; Lin, H.Q.; Ho, K.M.; Tringides, M. Metals on graphene: Interactions, growth morphology, and thermal stability. *Crystals* **2013**, *3*, 79–111. [CrossRef]
23. Ataca, C.; Aktürk, E.; Ciraci, S. Hydrogen storage of calcium atoms adsorbed ongraphene: First-principles plane wave calculations. *Phys. Rev. B* **2009**, *79*, 041406. [CrossRef]
24. Zhou, M.; Lu, Y.; Zhang, C.; Feng, Y.P. Strain effects on hydrogen storage capability of metal-decorated graphene: A first-principles study. *Appl. Phys.Lett.* **2010**, *97*, 103109. [CrossRef]
25. Banhart, F.; Kotakoski, J.; Krasheninnikov, A.V. Structural defects in graphene. *ACS Nano* **2010**, *5*, 26–41. [CrossRef] [PubMed]
26. Holmström, E.; Toikka, L.; Krasheninnikov, A.V.; Nordlund, K. Response of mechanically strained nanomaterials to irradiation: Insight from atomistic simulations. *Phys. Rev. B* **2010**, *82*, 045420. [CrossRef]
27. Lehtinen, O.; Kotakoski, J.; Krasheninnikov, A.V.; Tolvanen, A.; Nordlund, K.; Keinonen, J. Effects of ion bombardment on a two-dimensional target: Atomistic simulations of graphene irradiation. *Phys. Rev. B* **2010**, *81*, 153401. [CrossRef]
28. Alonso-Lanza, T.; Ayuela, A.; Aguilera-Granja, F. Substitutional 4*d* and 5*d* impurities in graphene. *Phys. Chem. Chem. Phys.* **2016**, *18*, 21913–21920. [CrossRef]
29. Sun, M.; Ren, Q.; Zhao, Y.; Chou, J.P.; Yu, J.; Tang, W. Electronic and magnetic properties of 4d series transition metal substituted graphene: A first-principles study. *Carbon* **2017**, *120*, 265–273. [CrossRef]
30. Wu, Z.; Cohen, R.E. More accurate generalized gradient approximation for solids. *Phys. Rev. B* **2006**, *73*, 235116. [CrossRef]
31. Vanderbilt, D. Soft self-consistent pseudopotentials in a generalized eigenvalue formalism. *Phys. Rev. B* **1990**, *41*, 7892–7895. [CrossRef] [PubMed]
32. Milman, V.; Lee, M.H.; Payne, M.C. Ground-state properties of $CoSi_2$ determined by a total-energy pseudopotential method. *Phys. Rev. B* **1994**, *49*, 16300. [CrossRef] [PubMed]
33. Payne, M.C.; Teter, M.P.; Allan, D.C.; Arias, T.A.; Joannopoulos, J.D. Iterative minimization techniques for ab initio total energy calculations: Molecular dynamics and conjugate gradients. *Rev. Mod. Phys.* **1992**, *64*, 1045–1097. [CrossRef]
34. Kresse, G.; Furthmuller, J. Efficient iterative schemes for ab initio total-energy calculations using a plane-wave basis set. *Phys. Rev. B* **1996**, *54*, 11169–11186. [CrossRef] [PubMed]
35. Monkhorst, H.J.; Pack, J.D. Special points for Brillouin-zone integrations—A reply. *Phys. Rev. B* **1977**, *16*, 1748.
36. Pfrommer, B.G.; Cote, M.; Louie, S.G.; Cohen, M.L. Relaxation of crystals with the quasi-newton method. *J. Comput. Phys.* **1997**, *131*, 133–140. [CrossRef]
37. Choi, S.M.; Jhi, S.H. Self-assembled metal atom chains on graphene nanoribbons. *Phys. Rev. Lett.* **2008**, *101*, 266105. [CrossRef]